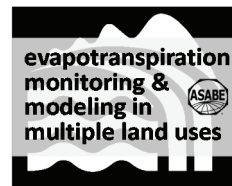


# THE VARIABILITY OF ASCE STANDARDIZED REFERENCE EVAPOTRANSPIRATION: A RIGOROUS, CONUS-WIDE DECOMPOSITION AND ATTRIBUTION



M. T. Hobbins

**ABSTRACT.** To fully attribute the variability of reference evapotranspiration to its drivers, a mean-value, second-moment uncertainty analysis is applied to a 30-year, CONUS-wide reanalysis of daily and annual tall-crop reference evapotranspiration as estimated by the ASCE Standardized Reference Evapotranspiration Equation driven by four variables from the North American Land Data Assimilation System phase 2 (NLDAS-2) reanalysis: temperature, specific humidity, wind speed, and downward shortwave radiation. The attribution methodology accounts for both the sensitivity of reference evapotranspiration to its drivers and their observed variabilities, and it permits the decomposition of reference evapotranspiration variability across CONUS at various timescales into contributions from each driver. An analytically derived expression of the sensitivity of daily ASCE Standardized Reference ET to each of the drivers is provided and mapped. Contrary to the assumption of much hydrologic practice, temperature is neither always nor everywhere the most significant driver of temporal variability in reference evapotranspiration. Instead, depending on regional hydroclimatology, season, and timescale, different drivers dominate; in fact, in many regions, temperature-based parameterizations should be avoided at all timescales.

**Keywords.** Attribution, Reference evapotranspiration, Uncertainty, Variability.

The concept of atmospheric evaporative demand is widely used across hydrological, agricultural, and climatological sectors as an upper limit in the estimation of actual evapotranspiration (ET); it represents ET freed from moisture constraints and subject instead only to the more analytically tractable advective and radiative constraints. Of the numerous metrics for evaporative demand, the earliest was the observation of evaporation from pans (later lysimeters), which Penman (1948) subsequently used to derive the concept of potential evaporation in an expression (the Penman equation) that first combined meteorological and radiative drivers. The Penman equation underpins the agriculturally focused Penman-Monteith (PM) concept (Monteith, 1965) of reference ET, which idealizes evaporative demand as the ET flux from a reference crop under strictly specified growing conditions. Traditionally, reference ET is used in irrigation scheduling to define a maximal ET from which field-scale crop ET, and hence crop irrigation requirements, are de-

rived according to crop type, growing cycle, and other factors. Reference ET has become the most widely used metric of evaporative demand; its estimation is codified internationally by the FAO-56 report (FAO, 1998) and for the U.S. by the ASCE Standardized Reference Evapotranspiration Equation (ASCE, 2005; hereafter referred to as “ASCE05”). A reanalysis-driven version of this ASCE05 reference ET is examined in this article.

## UNCERTAINTIES IN REFERENCE EVAPOTRANSPIRATION

Limiting epistemic uncertainties in the estimation of reference ET clearly has significant implications for irrigation scheduling but also in many other agricultural and water resource sectors, including drought monitoring, land surface modeling for, say, streamflow forecasting and reservoir management, and climate change impact assessments. Uncertainty arises from many sources: the choice of reference ET estimation method; the meteorological and/or radiative driving data, not only in their measurement but also from their spatial variability complicating interpolation between observation points; the selection of the most appropriate agrometeorological stations to represent a crop field’s climatic conditions; and the extent to which the assumption that surface, meteorological, or radiative conditions are representative of a reference crop is contravened. Crucially, modeling philosophies of estimators of evaporative demand in general and reference ET in particular have ranged from physically based estimators that model both radiative and advective dynamics (e.g., the PM model suit-

---

Submitted for review in September 2014 as manuscript number NRES 10975; approved for publication by the Natural Resources & Environmental Systems Community of ASABE in April 2015.

Mention of company or trade names is for description only and does not imply endorsement by the USDA. The USDA is an equal opportunity provider and employer.

The author is Michael T. Hobbins, Research Associate, Cooperative Institute for Research in Environmental Sciences, University of Colorado, and NOAA Earth System Research Laboratory, Physical Sciences Division (NOAA/ESRL/PSD), 325 Broadway, Boulder, CO 80305; phone: 303-497-3092; e-mail: mike.hobbins@noaa.gov.

able for estimation of actual ET, potential ET, and reference ET) to simpler models that rely on easily observed temperature either alone (e.g., the Thornthwaite (1948) and Hamon (1961) models of potential ET) or in combination with some parameterization of solar radiation (e.g., the Turc (1961) model of potential ET and the Blaney-Criddle (USDA, 1950), Jensen-Haise (Jensen and Haise, 1963), and Hargreaves (Hargreaves and Samani, 1985) models of reference ET). While the simpler, temperature-based approaches were developed for regions with incomplete atmospheric data where only a few driving parameters are measured and for timescales longer than daily, they either omit or only indirectly parameterize the influence of other physically appropriate drivers of variability of evaporative demand. Clearly, the selection of an appropriate suite of forcings for a model should balance the desire to reduce parameter uncertainty against the necessity of incorporating key sources of variability; ideally, parameter parsimony is conserved while physically representativeness is maintained. Finding this balance motivates this study.

#### REFERENCE EVAPOTRANSPIRATION REANALYSIS

The fundamental question this article seeks to answer is, “where, when, and to what extent do the meteorological and/or radiative inputs drive the spatial and temporal variability of reference ET?” To answer this question, and to fully describe how reference ET variability is derived from its drivers, a mean-value, second-moment uncertainty analysis is applied to NOAA’s 30-year, CONUS-wide dataset of daily, tall-crop reference ET (hereafter referred to as  $ET_r$ ) from ASCE05 with publically available, high-quality drivers from phase 2 of the North American Land Data Assimilation System (NLDAS-2; Mitchell et al., 2004). NOAA’s  $ET_r$  reanalysis is unique in its consistent modeling, low latency, and spatio-temporal extent. It is under development to represent reference ET’s variability as a spatially distributed complement to dense agrometeorological station networks, such as the Texas High Plains ET Network and the California Irrigation Management System, that are otherwise expensive alternatives of regionally limited extent. NOAA’s  $ET_r$  has been validated across western CONUS (Lewis et al., 2014) and the Texas High Plains (Moorhead et al., 2015), and while not yet deemed sufficiently accurate for the traditional use of  $ET_r$  in field-scale irrigation scheduling, it nonetheless remains a highly leveraged product with uses across many other agricultural and water resource sectors. For example, it is used in irrigation support in agriculture away from agrometeorological stations; for water resource managers charged with estimating landscape-scale actual ET such as the U.S. Geological Survey’s National Water Census for which it is under consideration (James Verdin, personal communication, 2015); as a climatology for the National Weather Service’s (NWS) Forecast Reference ET product (NWS, 2015); and in multiple monitoring and prediction activities, including underpinning an agricultural drought index (the Evaporative Demand Drought Index, EDDI; Hobbs et al., 2016) and to support the U.S. Forest Service’s seasonal forecasting of wildfire-suppression costs (Ham et al., 2014).

#### PREVIOUS SENSITIVITY ANALYSES

Previous studies have examined the sensitivity of reference ET to its drivers across a variety of hydroclimates and using a variety of formulations. For example, Saxton (1975) examined Penman-like equations at a daily timescale in western Iowa; Piper (1989) estimated the sensitivity of two monthly Penman-based formulations (Penman, 1963; Doorenbos and Pruitt, 1984) to input errors and parameter uncertainty at low-elevation stations, mostly in the tropics; Hupet and Vanclooster (2001) estimated errors in the FAO-56 equation due to sampling frequency in humid Belgium; Goyal et al. (2004) studied weekly driven PM estimates in an arid region in India; and Hou et al. (2013) examined the sensitivity of daily FAO-56 estimates in a desert oasis in western China. Perhaps the closest study to this study is that of Irmak et al. (2006), who conducted a sensitivity analysis of the daily ASCE05 equation at seven stations across a wide range of hydroclimates and elevations in CONUS. The primary conclusion from these studies is that the drivers dominating the sensitivity of reference ET vary according to hydroclimate and season.

While these studies have found great utility in the irrigated agriculture and agricultural science and planning communities, they mostly rely on the concept of non-dimensional relative sensitivity coefficients (McCuen, 1974) that does not account for the observed variability of the drivers; instead, they specify variations in the drivers regardless of whether these variations represent a sample of the driver’s historical population. However, if a driver varies little around its mean, the sensitivity of the response variable to it is moot. Nor does the concept allow for dependence between drivers, whereas, in fact, covariances between drivers can make significant contributions to the uncertainty or variability in a predicted variable by increasing, but often reducing, it. Many of these previous studies also express the humidity driver as a partial function of  $T$  (through relative humidity or vapor pressure deficit), so the influences of humidity and  $T$  cannot be distinguished. Further, all of these studies are station-based, either predating or choosing not to take advantage of the reanalyses datasets from which temporally and spatially extensive and fine-scale reference ET datasets may be derived. Most derive sensitivities from empirical relationships, while the preferred approach is to describe sensitivity through analytical expressions derived from differentiation of the driving equation (Saxton, 1975). While Saxton (1975), Piper (1989), and Hupet and Vanclooster (2001) used this preferred method, Hupet and Vanclooster (2001) did not publish the sensitivity expressions, and Saxton (1975) and Piper (1989) derived reference ET from Penman-like equations, not the ASCE05 reference ET that dominates the field today and that is used in this study.

#### RIGOROUS VARIABILITY ATTRIBUTION

The variability analysis described herein builds upon and improves the methodologies of these previous studies. As a member of the Method of Moments family of variability analysis techniques, it accounts for not only the sensitivity of reference ET to its drivers but also for the drivers’ observed variabilities and all covariances between them. It

permits the decomposition of the reference ET variability at various timescales into contributions from each driver. Because the driving data and predicted  $ET_r$  are spatially distributed across CONUS, the technique described herein covers a wide variety of hydroclimates. Further, sensitivity expressions are derived analytically (and provided and mapped).

Method of Moments techniques such as this have been used before to examine the variability of other varieties of evaporative demand. Fisher et al. (2005) assessed modeled evaporative demand across a wide range of simplicity of formulations and driver suites but assumed that the drivers were independent, i.e., that their covariances were negligible. The performance of these evaporative demand measures in then estimating ET depended on their specific formulations and driver sets, e.g., the performance of the Penman equation was highly sensitive to wind speed, while biases in some models were due solely to the inclusion of a single parameter (e.g., canopy stomatal resistance). Fisher et al. (2008) validated monthly remotely sensed evaporative demand-to-ET models against eddy covariance ground stations and found that net radiation (and not other meteorological or remotely sensed inputs) had the greatest impact on model accuracy. Fisher et al. (2005, 2008) also demonstrated the dangers of model over-complexity, as errors in estimating uncertain parameter sets are propagated through the models. Hobbins et al. (2012) applied the technique to a 30-year reanalysis of synthetic pan evaporation. Here, daily  $ET_r$  from the ASCE05 reference ET formulation (ASCE, 2005) as applied to a tall crop is examined, as it (and its short-grass equivalent) is the most commonly used estimator of evaporative demand.

In this article, a technique for decomposing the variability of ASCE05  $ET_r$  into the contributions from all of its drivers is fully described, including the provision of new analytical expressions for, and maps of, the sensitivity of ASCE05  $ET_r$  to its drivers that should find many uses and users. These expressions and the variability analysis framework are applicable to any input data to the ASCE05  $ET_r$ , regardless of their accuracy. The methodology and results of this variability analysis are outlined at various useful timescales, and the drivers of  $ET_r$  variability in space and time are demonstrated across CONUS, leading to a discussion of the implications for the estimation of reference ET in operational hydrology and climate change analyses.

## METHODOLOGY

In this section, the NOAA reference ET product is summarized, including the ASCE05 equation used; the Method of Moments variability analysis procedure is described; the specific sensitivity equations necessary for the analysis are provided; and a summation of the analysis is outlined.

### NOAA IMPLEMENTATION OF THE ASCE STANDARDIZED REFERENCE ET EQUATION

The ASCE Standardized Reference Evapotranspiration

Equation (ASCE, 2005) was derived from the Penman-Monteith concept (Monteith, 1965) as a weighted combination of radiative and advective forcings, but with the Penman wind function replaced by a series of resistances to diffusion of the water vapor from leaf stomates into the canopy and then from the canopy into the overpassing air (although these resistances are not explicit in ASCE05). As in all reference ET formulations, the ASCE05 equation estimates an idealized ET flux from a reference crop growing under strictly specified surface and moisture conditions: 0.5 m high alfalfa or 0.12 m short grass, well watered, actively growing, and completely shading the ground with an albedo of 0.23. In this study, we estimate tall-crop reference ET (or  $ET_r$ ).

The ASCE05 equation is well described in ASCE (2005). The specific form that NOAA uses for estimating  $ET_r$  at daily (or longer) timescales is as follows:

$$ET_r = \frac{0.408\Delta}{\Delta + \gamma(1 + C_d U)} (R_n - G) \frac{86400}{10^6} + \frac{\gamma C_n}{\Delta + \gamma(1 + C_d U)} T U \frac{(e_{sat} - e_a)}{10^3} \quad (1)$$

where  $ET_r$  is the tall-crop reference ET ( $\text{mm d}^{-1}$ );  $T$  is the 2 m air temperature (K);  $\Delta$  is the slope of the saturated vapor pressure curve at  $T$  ( $\text{Pa K}^{-1}$ );  $\gamma$  is the psychrometric constant ( $\text{Pa K}^{-1}$ );  $R_n$  is the net incoming radiation (sum of net shortwave and net longwave fluxes) at the surface ( $\text{W m}^{-2}$ );  $G$  is the downward ground heat flux ( $\text{W m}^{-2}$ ); the 86400/10<sup>6</sup> term converts  $R_n$  and  $G$  to the ASCE05-required units ( $\text{MJ m}^{-2} \text{d}^{-1}$ );  $U$  is the wind speed at 2 m above the surface ( $\text{m s}^{-1}$ );  $e_{sat}$  and  $e_a$  are the saturated and actual vapor pressures, respectively (Pa, converted to the ASCE05-required units of kPa by the 10<sup>3</sup> denominator);  $C_n$  and  $C_d$  are respectively the “numerator constant” ( $\text{K mm s}^3 \text{Mg}^{-1} \text{d}^{-1}$ ) and “denominator constant” ( $\text{s m}^{-1}$ ), with values defined in ASCE05; and the 0.408 term represents the inverse of the latent heat of vaporization ( $\text{m}^2 \text{mm MJ}^{-1}$ ), converting  $ET_r$  to depth units.

ASCE05  $ET_r$  is driven here by the following forcings: temperature at 2 m ( $T$ ), specific humidity at 2 m ( $q$ ), downward shortwave surface radiation ( $R_d$ ), and wind speeds at 10 m downscaled to 2 m wind speeds ( $U$ ) from NLDAS-2 (Mitchell et al., 2004). The purpose of NLDAS-2 is “to provide reliable initial land-surface states to coupled atmosphere-ocean-land models in an effort to improve weather predictions” (Xia et al., 2012). These forcings are available on an hourly basis from NOAA’s National Centers for Environmental Prediction. Before use in equation 1, they are converted to appropriate quantities: daily values for daily  $ET_r$  estimation, and annual daily mean values for annual  $ET_r$  estimation.

To estimate  $e_a$ , ASCE05 method 1 (table 3 in ASCE05) is used, wherein  $e_a$  is estimated as a daily average of hourly humidity estimates derived from  $q$  and station pressure  $P_a$  (same units as  $e_a$ ), as follows:

$$e_a = \frac{qP_a}{1 + 0.378q} \quad (2)$$

where  $P_a$  is an exponential function of station elevation (eq. 3 in ASCE, 2005).

To derive the daily wind speed data, hourly surface wind speeds are derived as the magnitudes of hourly orthogonal horizontal wind vector components UGRD10m ( $U_x$ ) and VGRD10m ( $U_y$ ) estimated by NLDAS-2 at 10 m above the ground and converted to the required 2 m wind speeds ( $U$ ) by accounting for the vertical wind speed profile, as follows:

$$U = \sqrt{U_x^2 + U_y^2} \frac{4.87}{\ln(67.8 \times 10 - 5.42)} \quad (3)$$

where the first term on the right side represents the scalar magnitude of the sum of  $U_x$  and  $U_y$  vectors, and the second term scales this to a 2 m elevation (eq. B.14b in ASCE05). Daily  $U$  is then derived as the daily arithmetical mean of hourly  $U$ .

$ET_r$  was then estimated from equation 1 for the period 1981 through 2010 across CONUS at a spatial resolution of 0.125°, at a daily timescale for the May-through-October (MJJASO) analysis and the daily-by-month analysis, and at an annual timescale (using annually averaged daily drivers) for the annual analysis. All subsequent analyses are conducted on these 30-year daily and annual  $ET_r$  reanalyses.

ASCE05-formulated  $ET_r$  driven by NLDAS-2 has been validated against agrometeorological stations across western CONUS (Lewis et al., 2014) and the Texas High Plains (Moorhead et al., 2015). Lewis et al. (2014) compared hourly NLDAS-2  $ET_r$  to that measured at 704 agrometeorological stations in the agricultural regions of the 17 westernmost states in CONUS. They found that the performance of drivers as measured against station observations decreased (in order) from  $T$  to  $R_d$  to RH to  $U$ , with unsatisfactory driver performance in several regions (the lowest  $r^2$  values were for  $U$  and RH in the intermountain west, for  $U$  in southern California, for  $R_d$  in Montana, and for  $T$  in southern Texas). They concluded that most arid environments had higher  $T$  and lower RH than would occur under the reference conditions assumed in the reference ET paradigm. However, the effects of unsatisfactory NLDAS-2 drivers were mitigated when applied in  $ET_r$ , which exhibited high correlations everywhere except Montana and western Washington and generally performed better in areas of low relief than in mountainous areas. The highest  $ET_r$  biases (i.e.,  $ET_r$  driven by NLDAS-2 exceeding station-based  $ET_r$ ) were in southern reaches of California, Arizona, New Mexico, and Texas, although systematic biases are less relevant to the outcome of this study than the fact that the variability in the  $ET_r$  derived from NLDAS-2 matched well with that derived from the station-based data (i.e., high  $r^2$ ).

Moorhead et al. (2015) validated NOAA's  $ET_r$  against daily  $ET_r$  measured for ten years at 14 agrometeorological stations in the Texas High Plains Evapotranspiration (TXHPET) network. NOAA  $ET_r$  were strongly correlated with the TXHPET data ( $r^2$  varied from 0.79 to 0.82, with all stations reporting significant relations at  $p < 0.0001$ ) but were positively biased (NOAA  $ET_r$  overestimated TXHPET  $ET_r$ ), primarily due to overestimations of  $T$  and  $U$ .

Lewis et al. (2014) and Moorhead et al. (2015) both concluded that the current generation of NOAA's  $ET_r$  reanalysis is not sufficiently accurate for the traditional use of  $ET_r$  (field-scale irrigation scheduling) for two primary reasons: (1) the spatial resolution is insufficient for field-scale operations, and (2) the contravention of the surface assumptions of reference ET, whereby the land surface is too dry and thus the temperature, humidity, and wind speed drivers do not represent those that would exist over the reference surface assumed in the reference ET paradigm. Nevertheless, NOAA's  $ET_r$  reanalysis remains useful in many other agricultural and water resource sectors, as indicated earlier.

Figure 1 shows the mean and variability (or variance) of  $ET_r$  across the 30-year reanalysis period for two of the timescales and timeframes examined in the results: daily  $ET_r$ , pooled across the warm MJJASO period, and annual  $ET_r$ . (Hereafter, "timescale" refers to the time step at which the  $ET_r$  model is run, and "timeframe" refers to the period across which the analysis is conducted, e.g., daily  $ET_r$  examined across October is at a daily timescale but a monthly timeframe.) While the mean daily  $ET_r$  for MJJASO generally exceeds the annual rate by about 2 mm d<sup>-1</sup>, both maps share similar features. As expected,  $ET_r$  is highest in the sunniest, warmest, driest, and windiest regions of CONUS, so both range from maxima in the Southwest to minima in the Northeast, and both decline with increasing local elevation.

The mean maps are more similar across timeframes than are the variability maps, but there is little similarity between each timeframe's mean and corresponding variability maps. The MJJASO daily variabilities are an order of magnitude higher than the annual variabilities. While both MJJASO daily  $ET_r$  and annual  $ET_r$  are highly variable across the High Plains, the northern High Plains regional maximum of daily MJJASO variability is shifted to the north and west (Montana, North Dakota, and South Dakota) relative to that in the annual variability (South Dakota, Nebraska, Iowa). There is also a regional variability maximum in daily MJJASO variability across the desert southwest (southern Nevada and Utah) and Pacific Northwest (Washington, northern Oregon) not present in the annual pattern. Although not shown here, there is also significant monthly change of variability in daily  $ET_r$ . The area of greatest variability in January is limited to Texas and eastern New Mexico, whereas the greatest variability in July is found in the High Plains.

The next section describes the decomposition of these  $ET_r$  variabilities at different timeframes into contributions from the four drivers of  $ET_r$  ( $T$ ,  $q$ ,  $R_d$ , and  $U$ ).

## MEAN-VALUE, SECOND-MOMENT VARIABILITY ANALYSIS

The variability in a hydrologic response (or model output) results from driver variabilities that propagate through the physical process (or model). We seek a technique to quantify the relative effects of each driver's variability on the predicted variable  $ET_r$ . As we are only interested in decomposing the variance (the second moment) of the output ( $ET_r$ ), we use a first-order, second-moment (FOSM)

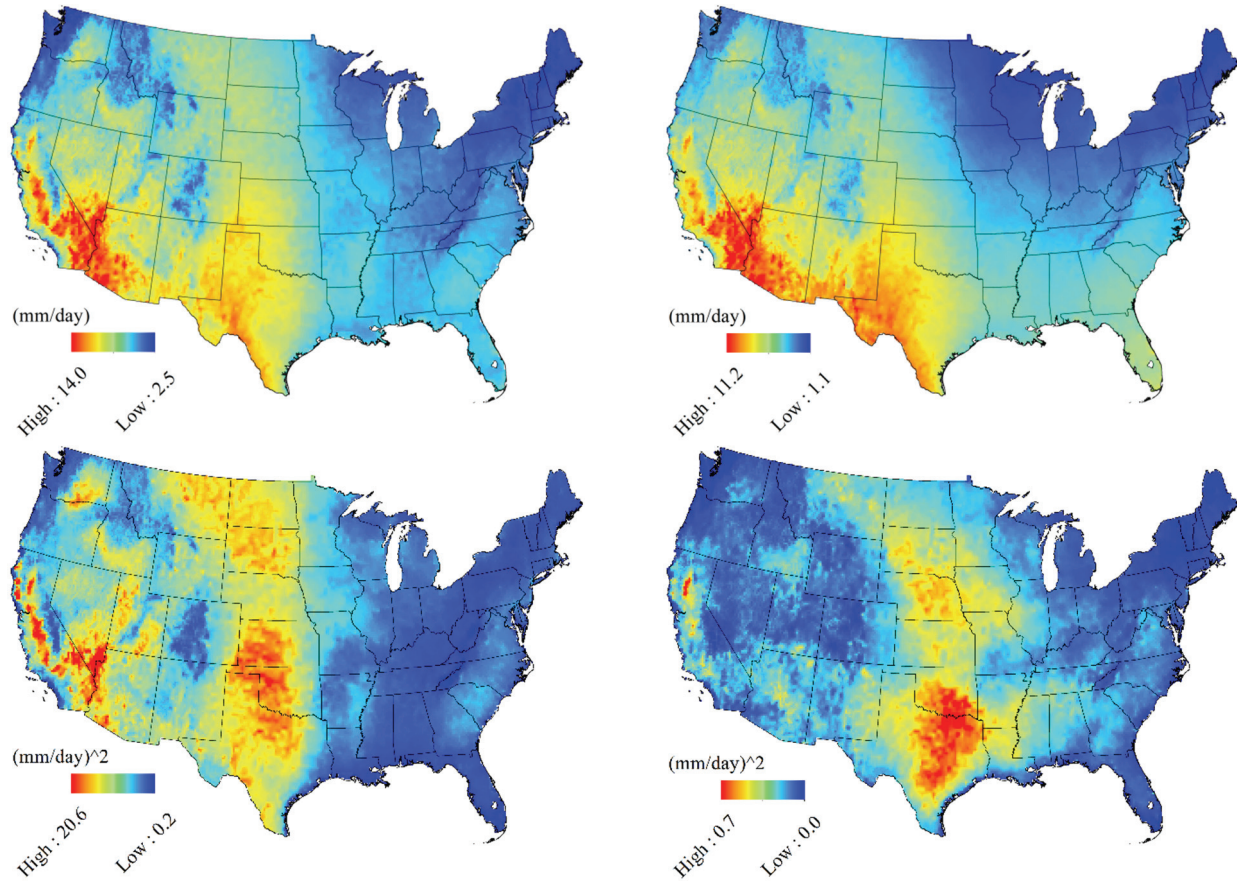


**Figure 1.** Thirty-year means (top row; mm d<sup>-1</sup>) and variabilities (bottom row; mm<sup>2</sup> d<sup>-2</sup>) of ET<sub>r</sub> across various timescales and timeframes: (left) daily ET<sub>r</sub> pooled across MJJASO and (right) annually modeled ET<sub>r</sub>. Note that a different range applies to each map.

analysis of variability, which foregoes knowledge of the driving parameters' distributions in favor of describing their variability by their means (for central tendencies) and variances (for their spread around the mean). FOSM yields reasonable approximations given that drivers' variations around their means are uniformly distributed and small and also that the formulation of the model (i.e., the ET<sub>r</sub> equation from eq. 1) is only mildly nonlinear. Given that these

The following discussion describes the FOSM technique, in which a specific functional relationship,  $f(X_i, i = 1 \dots n)$ , is assumed between all  $n$  drivers  $X_i$  and a model output (ET<sub>r</sub> from eq. 1), and then the response variability is attributed to each driver. As ET<sub>r</sub> is a function of the four drivers, i.e.,  $ET_r = f\{T, q, R_d, U\}$ , which are assumed random variables, the variability in ET<sub>r</sub> ( $\sigma_{ET_r}^2$ ) may be described as shown in equation 4.

$$\sigma_{ET_r}^2 = F_T + F_q + F_{R_d} + F_U = \left\{ \begin{aligned} & \left( \frac{\partial ET_r}{\partial T} \right)^2 \sigma_T^2 + \frac{\partial ET_r}{\partial T} \frac{\partial ET_r}{\partial q} \sigma_{T,q} + \frac{\partial ET_r}{\partial T} \frac{\partial ET_r}{\partial U} \sigma_{T,U} + \frac{\partial ET_r}{\partial T} \frac{\partial ET_r}{\partial R_d} \sigma_{T,R_d} \\ & + \left( \frac{\partial ET_r}{\partial q} \right)^2 \sigma_q^2 + \frac{\partial ET_r}{\partial q} \frac{\partial ET_r}{\partial T} \sigma_{q,T} + \frac{\partial ET_r}{\partial q} \frac{\partial ET_r}{\partial U} \sigma_{q,U} + \frac{\partial ET_r}{\partial q} \frac{\partial ET_r}{\partial R_d} \sigma_{q,R_d} \\ & + \left( \frac{\partial ET_r}{\partial R_d} \right)^2 \sigma_{R_d}^2 + \frac{\partial ET_r}{\partial R_d} \frac{\partial ET_r}{\partial T} \sigma_{R_d,T} + \frac{\partial ET_r}{\partial R_d} \frac{\partial ET_r}{\partial q} \sigma_{R_d,q} + \frac{\partial ET_r}{\partial R_d} \frac{\partial ET_r}{\partial U} \sigma_{R_d,U} \\ & + \left( \frac{\partial ET_r}{\partial U} \right)^2 \sigma_U^2 + \frac{\partial ET_r}{\partial U} \frac{\partial ET_r}{\partial T} \sigma_{U,T} + \frac{\partial ET_r}{\partial U} \frac{\partial ET_r}{\partial q} \sigma_{U,q} + \frac{\partial ET_r}{\partial U} \frac{\partial ET_r}{\partial R_d} \sigma_{U,R_d} \end{aligned} \right\} \quad (4)$$

assumptions are not contravened and that there are few driving parameters (four in our case), FOSM requires less computational effort than other uncertainty analyses, such as Monte Carlo simulation (Mishra, 2009).

The rows in the bracketed term on the right side of equation 4 represent the contributions to  $\sigma_{ET_r}^2$  from each of the drivers ( $F_T$ ,  $F_q$ ,  $F_{R_d}$ , and  $F_U$ , respectively). Each row may be expressed more succinctly for a notional driver  $X$  drawn

from the suite of drivers as:

$$F_X \stackrel{\text{def}}{=} \left( \frac{\partial ET_r}{\partial X} \right)^2 \sigma_X^2 + \frac{\partial ET_r}{\partial X} \sum_{i=1}^3 \left( \frac{\partial ET_r}{\partial Y_i} \sigma_{X,Y_i} \right) \quad (5)$$

where the first term on the right side represents the contribution of variabilities in the individual driver  $X$  varying independently, and the second term represents the contribution from the interdependence of all possible pairs of drivers  $\{X, Y\}$ , where  $Y_i$  is the  $i$ th of the three drivers other than  $X$ .

Note that the first term in each bracketed line of equation 4 (or the first term on the right side of eq. 5) is always positive, i.e., the variability in the driver considered alone always augments the variability in  $ET_r$ . However, due to the presence of the covariance term ( $\sigma_{X,Y_i}$ ), the remaining terms in each line of equation 4 (or the second term on the right side of eq. 5) may often be negative. Thus, even if the sensitivity to each of the drivers ( $\partial ET_r / \partial X$ ) is always positive (i.e.,  $ET_r$  increases for an increase in the driver), two drivers may covary in such a way as to decrease the variability in  $ET_r$ . For instance, in the Southern High Plains,  $ET_r$  is positively sensitive to both  $U$  and  $q$  (fig. 2), yet these two drivers exhibit negative covariance (fig. 3); thus,  $U$  and  $q$  each separately increase variability in  $ET_r$ , but together their interactions tend to decrease  $ET_r$  variability, and the latter effect may exceed the former. In fact, it will be

shown that in some regions at some timescales, the overall effect of some variables is to reduce variability in  $ET_r$ . It is for this reason that the following maps often indicate negative contributions to  $ET_r$  variability or positive contributions above 100% of the total  $ET_r$  variability; across the four drivers, the contributions will always sum to 100%.

#### APPLYING VARIABILITY ANALYSIS TO THE $ET_r$ REANALYSIS DATASET

Following Saxton (1975), the expressions for the sensitivities of  $ET_r$  to its drivers ( $\partial ET_r / \partial X$ ) are derived analytically from an expression for  $ET_r$  that is differentiable with respect to each driver. Equation 6 is equation 1 reformulated in explicit terms of the four drivers; all other terms are either constants, i.e.,  $C_n$ ,  $C_d$ , height of wind speed measurement  $z_m$  (m), shortwave albedo ( $\alpha$ ), and Stefan-Boltzmann constant  $\sigma$  ( $W m^{-2} K^{-4}$ ), or parameters whose values are fixed for a fixed point in space ( $P_a$ ,  $\gamma$ ) or space and time (clear sky radiation  $R_{so}$  ( $W m^{-2}$ ), defined by equation 19 in ASCE05). To derive the sensitivity of  $ET_r$  to each driver  $X$ , equation 6 is partially differentiated with respect to  $X$ . These sensitivities are shown for  $T$ ,  $q$ ,  $R_d$ , and  $U$ , respectively, in equations 7 to 10, with simplifications used for derived quantities that are functions of only one driver (e.g.,  $e_{sat}$  is used where appropriate, as it varies solely as a function of  $T$ ).

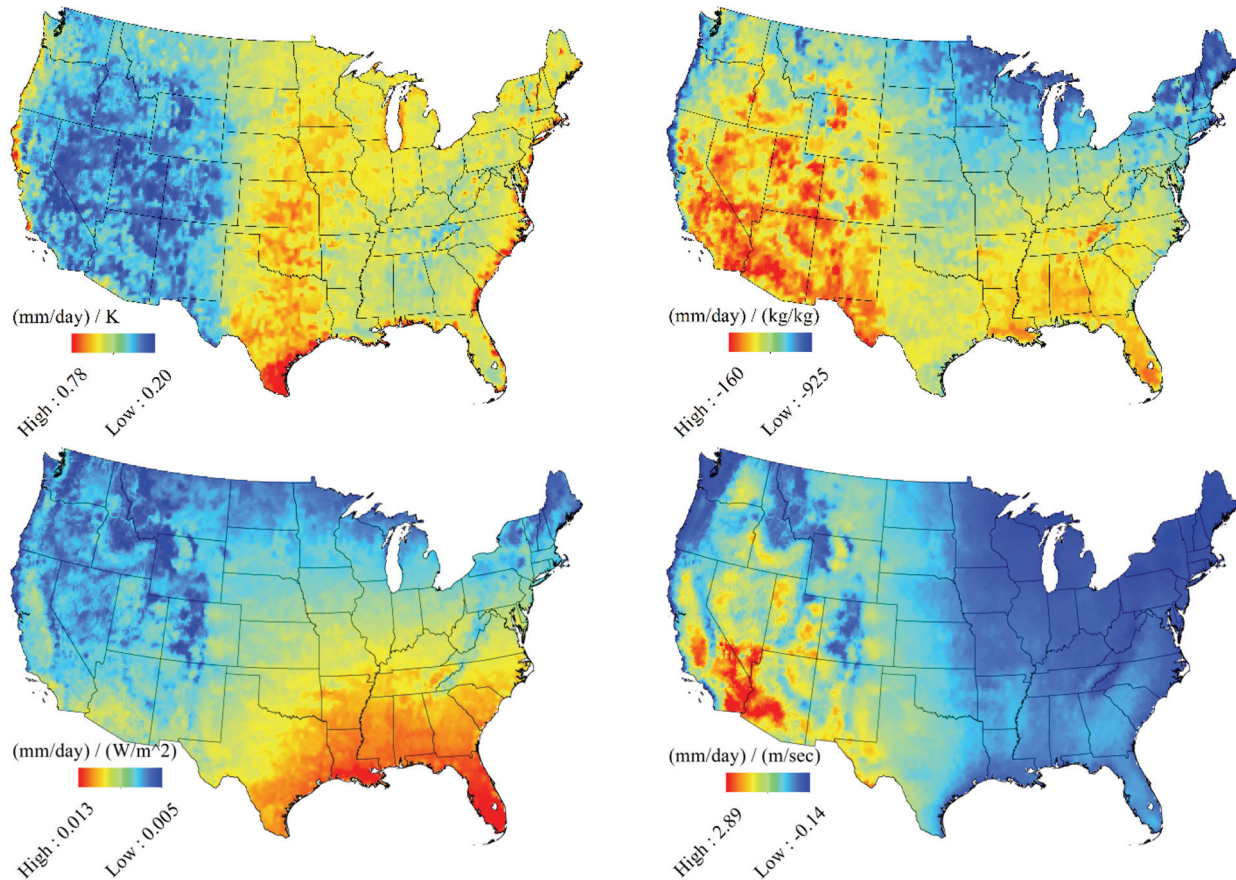


**Figure 2. Sensitivity ( $\partial ET_r / \partial X$ ) of daily  $ET_r$  across MJJASO to each of its drivers (left to right, top to bottom):  $\partial ET_r / \partial T$ ,  $\partial ET_r / \partial q$ ,  $\partial ET_r / \partial R_d$ , and  $\partial ET_r / \partial U$ . Note that each map has different units.**

$$ET_r = \frac{\left\{ 0.408 \times 2503 \frac{\exp\left(\frac{17.27(T-273.15)}{T-35.85}\right)}{(T-35.85)^2} \left[ (1-\alpha)R_d - \sigma \left( 1.35 \frac{R_d}{R_{so}} - 0.35 \right) \left( 0.34 - 0.14 \sqrt{\frac{qP_a}{0.622+0.378q}} T^4 \right) \right] + \gamma \frac{C_n}{T} U \left[ 0.6108 \exp\left(\frac{17.27(T-273.15)}{T-35.85}\right) - \frac{qP_a}{0.622+0.378q} \right] \right\}}{2503 \frac{\exp\left(\frac{17.27(T-273.15)}{T-35.85}\right)}{(T-35.85)^2} + \gamma(1+C_dU)} \quad (6)$$

$$\frac{\partial ET_r}{\partial T} = \frac{\left\{ 0.408\bar{\Delta} \left[ \bar{R}_n \frac{4169.871-2\bar{T}}{(\bar{T}-35.85)^2} - 4\sigma f_{cd} (0.34 - 0.14\sqrt{\bar{e}_a})\bar{T}^3 \right] + \gamma C_n \frac{\bar{U}}{\bar{T}} \left[ \bar{e}_{sat} \frac{4098.171}{(\bar{T}-35.85)^2} - \frac{1}{\bar{T}} (\bar{e}_{sat} - \bar{e}_a) \right] \right\}}{\bar{\Delta} + \gamma(1+C_d\bar{U})} + \frac{\frac{4169.871-2\bar{T}}{(\bar{T}-35.85)^2} \bar{\Delta} \left[ 0.408\bar{\Delta} \bar{R}_n + \gamma \frac{C_n}{\bar{T}} \bar{U} (\bar{e}_{sat} - \bar{e}_a) \right]}{\bar{\Delta} + \gamma(1+C_d\bar{U})^2} \quad (7)$$

$$\frac{\partial ET_r}{\partial q} = 0.622 P_a \frac{0.02856 \bar{\Delta} \sigma f_{cd} \bar{T}^4 \frac{1}{\sqrt{\bar{e}_a}} - \gamma \frac{C_n}{\bar{T}} \bar{U}}{[\bar{\Delta} + \gamma(1+C_d\bar{U})](0.622+0.378q)^2} \quad (8)$$

$$\frac{\partial ET_r}{\partial R_d} = 0.408 \bar{\Delta} \frac{1-\alpha-\sigma \frac{1.35}{R_{so}} (0.34 - 0.14\sqrt{\bar{e}_a})\bar{T}^4}{\bar{\Delta} + \gamma(1+C_d\bar{U})} \quad (9)$$

$$\frac{\partial ET_r}{\partial U} = \gamma \frac{[\bar{\Delta} + \gamma(1+C_d\bar{U})] \frac{C_n}{\bar{T}} (\bar{e}_{sat} - \bar{e}_a) - C_d [\bar{\Delta} + \gamma(1+C_d\bar{U})] \bar{U} (\bar{e}_{sat} - \bar{e}_a)}{[\bar{\Delta} + \gamma(1+C_d\bar{U})]^2} \quad (10)$$

These sensitivity expressions are evaluated at the four drivers' means across the timeframe of interest, as indicated by the overbars. For instance, the  $\bar{e}_{sat}$  term is derived as follows:

$$\bar{e}_{sat} = 0.6108 \exp\left(\frac{17.27(\bar{T}-273.15)}{\bar{T}-35.85}\right) \quad (11)$$

where  $\bar{T}$  is estimated from:

$$\bar{T} = \frac{1}{30 \times 184} \sum_{y=1981}^{2010} \sum_{d=\text{May}1}^{\text{Oct}31} T_{Y,D} \quad (12)$$

which represents the daily mean  $T$  across the 184-day ( $D$ ) MJASO period for all 30 years ( $Y$ ) in the ET<sub>r</sub> reanalysis. For daily ET<sub>r</sub> across MJASO, the population from which all means, variances, and covariances are estimated consists of all days from May 1 to October 31 across the period 1981 to 2010 ( $n = 5520 = 30 \text{ years} \times 184 \text{ days}$ ), while for annually estimated ET<sub>r</sub>, the population consists of mean annual ET<sub>r</sub> across the period 1981 to 2010 ( $n = 30 \text{ years}$ ).

These sensitivities are mapped across CONUS for daily MJASO ET<sub>r</sub> in figure 2. The variance ( $\sigma^2_X$ ) and covariance ( $\sigma_{X,Y}$ ) terms in equations 4 and 5 are evaluated empiri-

cally from the dataset. Maps of the variance of each driver are shown in figure 3, and maps of the covariances between all drivers are shown in figure 4.

#### ASSESSING RELATIVE CONTRIBUTIONS OF EACH DRIVER TO OVERALL ET<sub>r</sub> VARIABILITY

Equation 4 is then evaluated at each pixel across CONUS, and the relative contribution of each driver  $X$  ( $B_X$ , %) to the overall ET<sub>r</sub> variability is estimated by comparing the contributions  $F_X$  to the total ET<sub>r</sub> variability, as follows:

$$B_X \stackrel{\text{def}}{=} \frac{F_X}{\sum_{x=1}^4 F_x} \times 100 \quad (13)$$

Note that  $B_X$  is not constrained to lie between 0% and 100% due to negative contributions to ET<sub>r</sub> variability that may arise due to the effects of the negative covariance terms, as discussed previously.

The relative contributions ( $B_X$ ) are mapped across CONUS for daily MJASO ET<sub>r</sub> in figure 5 and for annual ET<sub>r</sub> in figure 9. They are ranked for daily MJASO ET<sub>r</sub> in figure 6. The driver with the greatest contribution is mapped for daily MJASO ET<sub>r</sub> in figure 7, for daily ET<sub>r</sub> by each month in figure 8, and for annual ET<sub>r</sub> in figure 10.

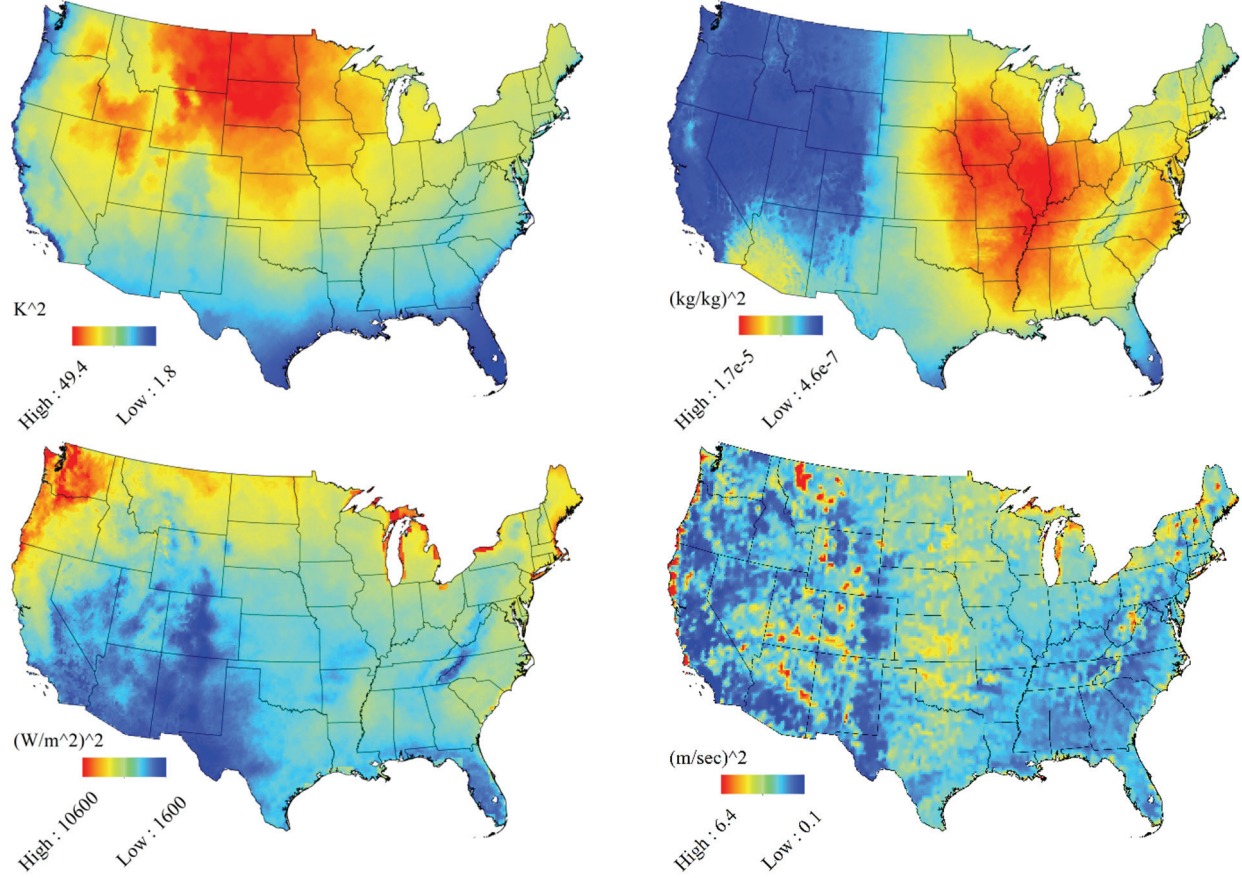


**Figure 3.** Variances ( $\sigma^2_x$ ) of daily  $ET_r$  drivers across MJJASO (left to right, top to bottom):  $\sigma^2_T$ ,  $\sigma^2_q$ , and  $\sigma^2_{R_d}$ , and  $\sigma^2_U$ . Note that each map has different units.

## RESULTS

The methodology described in the preceding section was applied to the NOAA ET<sub>r</sub> dataset for 1981–2010 at a variety of timescales and timeframes to examine the dynamic nature of the variability of ET<sub>r</sub> across CONUS. First, daily variability is examined across the warm MJJASO period (used here to approximate the growing season for the sake of consistency across the continental extent of this study), thereby fully demonstrating the methodology at the timescale and timeframe most useful to agriculturalists. The decomposition of daily ET<sub>r</sub> variability is then summarized at a finer, monthly timeframe. Finally, as a counterpoint context that is more useful to climatologists, annual ET<sub>r</sub> variability is examined. As a reminder, the following results refer to the variability in ET<sub>r</sub> around its mean and what drives it, not to the magnitude of ET<sub>r</sub>.

### DAILY ET<sub>r</sub> VARIABILITY ACROSS THE WARM SEASON (MJJASO)

Figure 2 maps the sensitivities of daily ET<sub>r</sub> across MJJASO to each of its drivers ( $\partial ET_r / \partial X$ , derived from eqs. 7 to 10), where each over-barred driver in the expressions is evaluated at its mean across 30 years of daily ET<sub>r</sub> from May 1 to October 31. There is a clear, strong elevational signal in  $\partial ET_r / \partial R_d$  and  $\partial ET_r / \partial U$ , with mountain ranges discernible where the sensitivity to both drivers declines;  $\partial ET_r / \partial T$  appears opposite in pattern to  $\partial ET_r / \partial q$  and  $\partial ET_r / \partial R_d$  (it is lower

in western CONUS and higher in the east), while  $\partial ET_r / \partial q$  and  $\partial ET_r / \partial R_d$  also exhibit negative latitudinal gradients in eastern CONUS (highest around the Gulf of Mexico). The highest  $\partial ET_r / \partial U$  occurs in the desert Southwest.

Figure 3 maps the variances  $\sigma^2_x$  of the four NLDAS-2 drivers of daily ET<sub>r</sub> across MJJASO. The variances  $\sigma^2_T$ ,  $\sigma^2_q$ , and  $\sigma^2_{R_d}$  display a smooth texture and broad geographic patterns across CONUS:  $\sigma^2_T$  shows regional maxima in the continental interior, greatest in the northern Great Plains (North Dakota, South Dakota, and eastern Montana and Wyoming) and decreasing toward the south and the Atlantic and Pacific Coasts;  $\sigma^2_q$  shows a maximum across the Midwest and Mississippi valley and significantly lower values across the western third of CONUS, with the exception of regional maxima in the desert Southwest (southern California and Arizona) and the mid-Atlantic states east of the Piedmont; and  $\sigma^2_{R_d}$  has maxima in the Pacific Northwest and the Great Lakes' immediate borders and is lowest in Florida, the Southwest, and the Appalachian Mountains. In contrast,  $\sigma^2_U$  is both patchy in texture (presumably from a heavy station-based influence in the NLDAS-2 assimilation procedures for  $U_x$  and  $U_y$  observations) and much less geographically coherent. This is particularly evident across western CONUS, where  $\sigma^2_U$  appears bimodal, with a generally low background value interrupted by patches of much higher values. Maximal  $\sigma^2_U$  values appear around the Great Lakes' immediate borders. This patchy texture of  $\sigma^2_U$

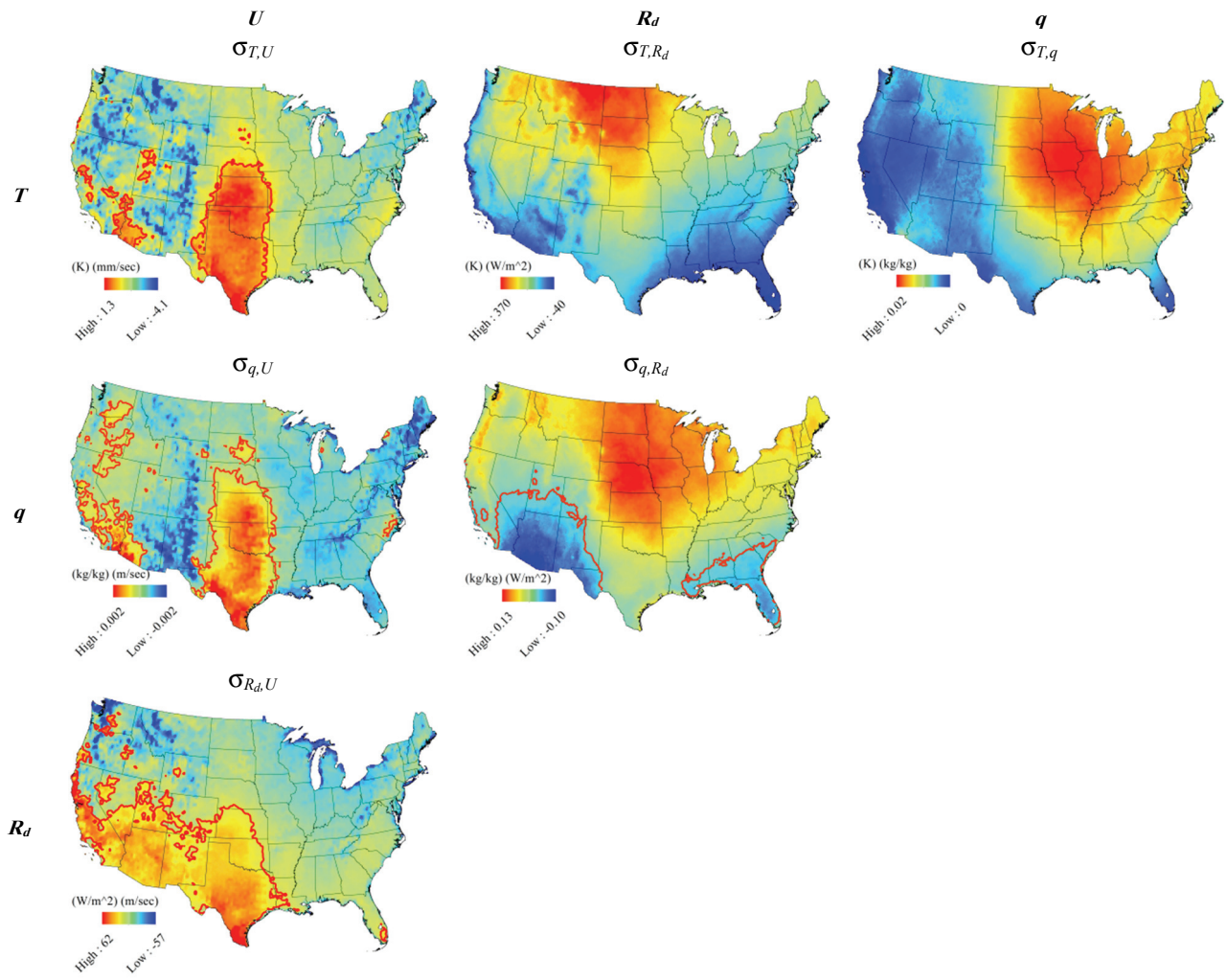


Figure 4. All covariances of drivers of daily  $ET_r$  pooled across 1981–2010 MJJASO. Red lines are contours of zero covariance. Note that each map has different units, and commutatively identical covariances are not shown (e.g.,  $\sigma_{q,T}$  is not shown, as it is identical to  $\sigma_{T,q}$ ).

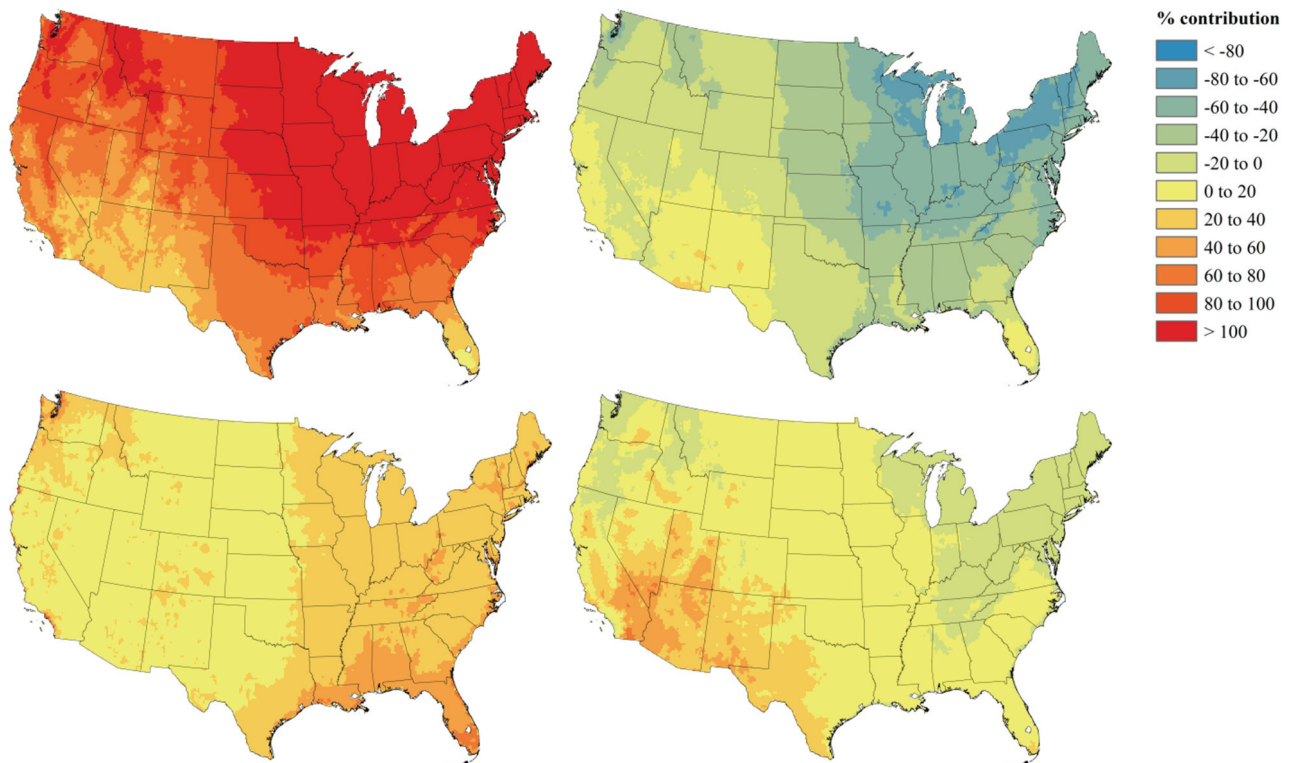
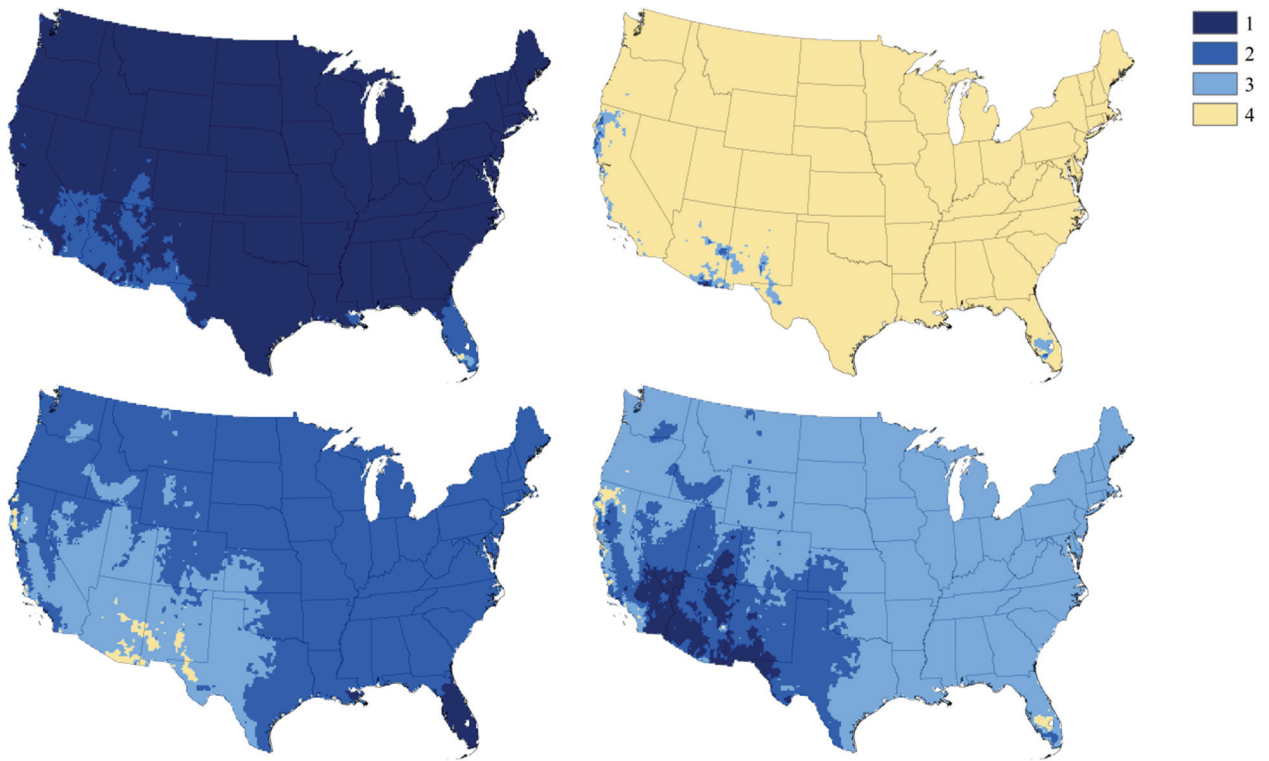
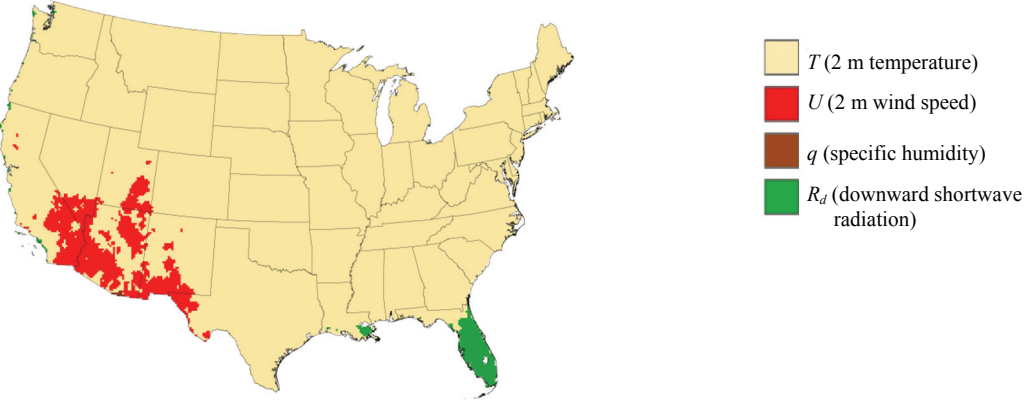


Figure 5. Relative contributions ( $B_x$ , %) of each driver to daily  $ET_r$  variability across MJJASO (left to right, top to bottom):  $T$ ,  $q$ ,  $R_d$ , and  $U$ .



**Figure 6.** Rank of each driver's contribution ( $B_x$ ) to daily  $ET_r$  variability across MJJASO (left to right, top to bottom):  $T$ ,  $q$ ,  $R_d$  and  $U$ .



**Figure 7.** Dominant drivers of daily  $ET_r$  variability across MJJASO. The top-ranked driver is indicated by color.

is also reflected in all  $\sigma^2_{U,Y}$  covariance maps (fig. 4).

Figure 4 maps the daily MJJASO covariance terms ( $\sigma_{X,Y}$ ) used in the variability decomposition. Note that many covariance maps have negative and positive values; as stated previously, this means that these terms may augment  $ET_r$  variability (in the case of positive covariance) and reduce it (in the case of negative covariance). Depending on region,  $R_d$  covaries negatively with  $q$  and/or  $U$ , while  $U$  covaries positively and negatively with all other variables. Of particular interest here is that although  $T$  and  $R_d$  covary positively across almost all of CONUS at this timeframe, this is due to the strong seasonal signal in both variables. At the monthly timeframe (not shown), they covary negatively over much of CONUS in summer; this refutes the underlying assumption of  $T$ -based formulations of evaporative demand (Hobbins et al., 2012), which is that the positive  $T\text{-}R_d$  covariance allows modelers to use  $T$  as a proxy for  $R_d$  due

to surface heating following clearer skies and cooling from increased cloud cover. Clearly, the assumption does not hold in regions or seasons of negative  $T\text{-}R_d$  covariance, such as for many months in the southeastern CONUS, which is also the region of highest variability of  $R_d$ .

The relative contribution to  $ET_r$  variability of each driver ( $B_x$  from eq. 13) is mapped in figure 5. Where  $B_T$  is highest,  $B_q$  is lowest, meaning that the effect of  $T$ 's positive contribution to increased  $ET_r$  variability is mitigated by  $q$ , which reduces  $ET_r$  variability.  $B_U$  is high where neither  $B_T$  nor  $B_q$  is high (neither positive nor negative), as in the Southwest and peninsular Florida.  $B_{R_d}$  has a longitudinal gradient and is generally higher (positive) in eastern CONUS than western (but is also high in the Pacific Northwest).  $B_T$  is highest in the Great Lakes region, peaking above 150% in northern Wisconsin and upstate New York, Pennsylvania, Vermont, and New Hampshire, and

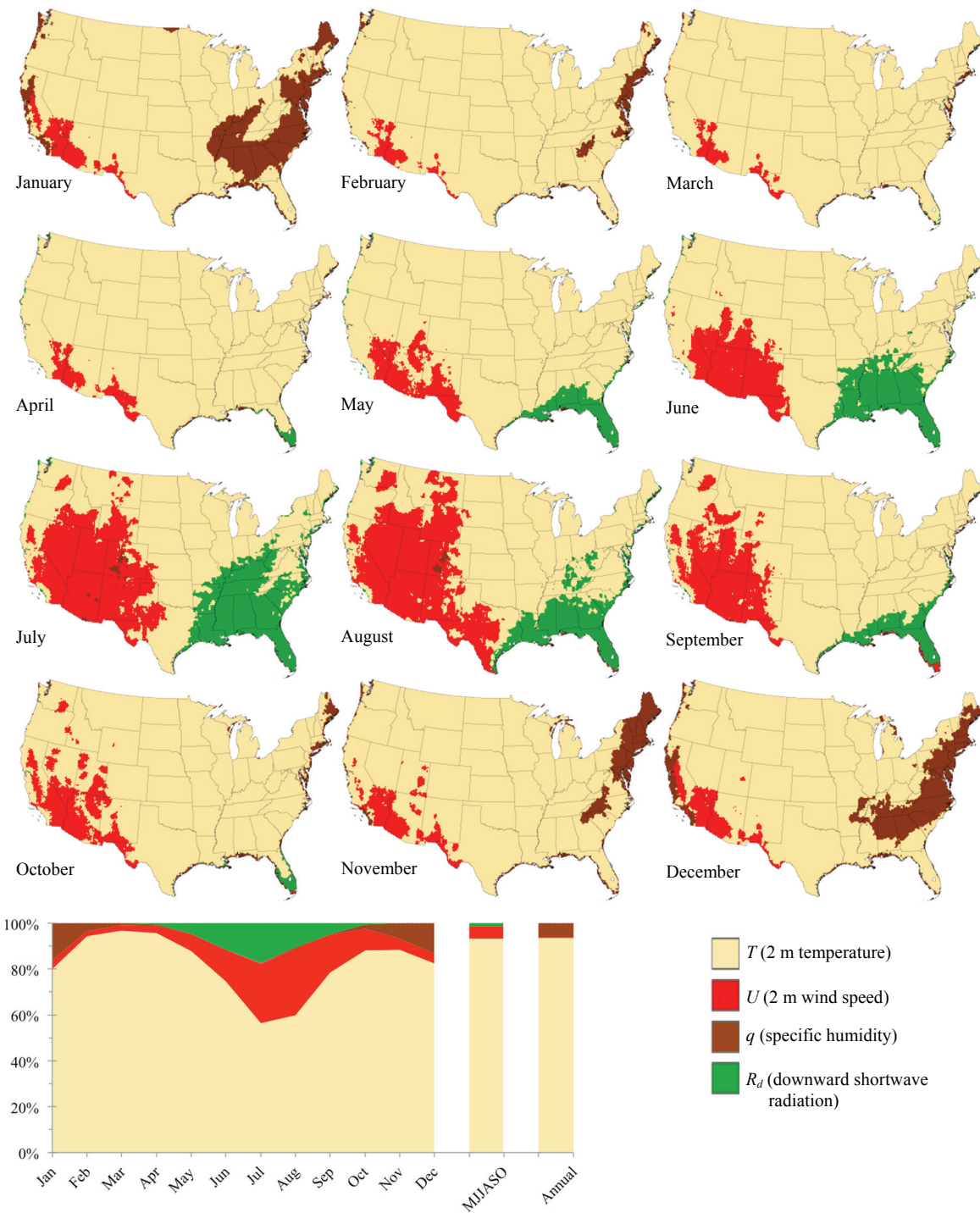


**Figure 8. Dominant drivers of daily  $ET_r$  variability for each month. The top-ranked driver is indicated by color. The graph shows the percentage of CONUS area over which each driver dominates (i.e., is top-ranked) for daily monthly data and for daily MJJASO and annual data.**

reaching a low of ~0% in the desert Southwest, along the Gulf Coast, and in Florida.  $B_q$  shows almost an inverse relationship to  $B_T$ . It is lowest around the Great Lakes (CONUS minimum of < -75% in northern Wisconsin and upstate New York, Pennsylvania, Vermont, and New Hampshire) and highest in the Southwest (CONUS maximum of > 31%) and in southern Florida.  $B_{R_d}$  is very low in western CONUS, reaching below 10% in parts of the western interior. It exceeds 20% everywhere across eastern CONUS,

where it exhibits a negative latitudinal gradient (reaching 60% in southern Florida).  $B_U$  is highest in the Southwest (CONUS maximum of 74% in southern interior California) and lower than 10% almost everywhere else across CONUS, with the lowest contributions in the Appalachian Range, the Olympic Peninsula (CONUS minimum of -10%), and the Cascade Range.

Figure 6 shows  $B_X$  (the relative contribution to  $ET_r$  variability) ranked for each driver across CONUS. Immediately

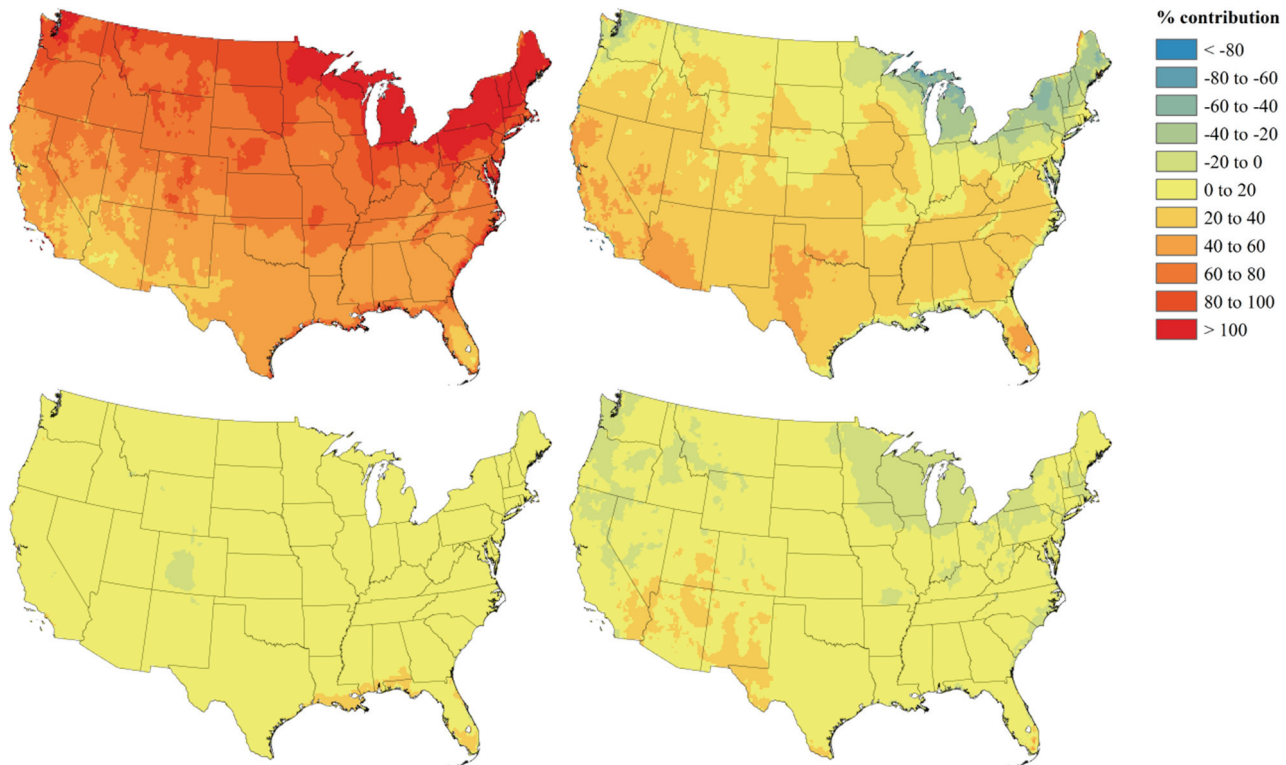


**Figure 9.** Relative contribution ( $B_X$ , %) of each driver to annual  $ET_r$  variability (left to right, top to bottom):  $T$ ,  $q$ ,  $R_d$ , and  $U$ .



**Figure 10.** Dominant drivers of annually modeled  $ET_r$  variability. The top-ranked driver is indicated by color.

clear is that, at the daily timescale across MJASO,  $T$  is almost uniformly ranked first across CONUS, with notable exceptions in the desert Southwest, where it is ranked second, and in peninsular Florida, where its rank falls to second through fourth. In contrast,  $q$  is ranked last almost everywhere, with a few patchy exceptions in northern coastal California, southern Arizona, New Mexico and western Texas, and southern Florida, where it is generally ranked third. The ranks of  $R_d$  and  $U$  reflect the southwestern exception evident in the  $B_T$  map (fig. 5).  $R_d$  attains first rank in energy-limited peninsular Florida but falls to third and fourth rank in the water-limited Southwest.  $U$  has the reverse pattern, being ranked first in the desert Southwest, second across the rest of the Southwest and southern High Plains, and falling to third across the rest of CONUS (except southern Florida, where  $U$  falls to fourth rank,  $q$  rises from fourth to third rank, and  $R_d$  dominates).

Figure 7 summarizes the results in figure 6 by indicating just the top-ranked driver across CONUS. Clear here is the dominance of  $T$  in driving daily  $ET_r$  variability across the warm season as a whole, while  $U$  dominates in the desert Southwest, and  $R_d$  dominates in peninsular Florida.

#### TOP-RANKED DRIVERS OF DAILY $ET_r$ VARIABILITY BY MONTH

Analysis of daily  $ET_r$  variability at the super-seasonal timeframe used in the preceding section overemphasizes the power of strongly seasonal drivers such as  $T$ ; thus, in this section, daily  $ET_r$  variability is decomposed at a monthly timeframe (i.e., daily  $ET_r$  binned into each month).

At first glance, figure 8 appears to show  $T$  dominating the variability of daily  $ET_r$  by month (i.e.,  $B_T$  is top-ranked); however, at no time does a single driver dominate everywhere. Likewise, in very few regions is there a single

dominant driver every month. Instead, the dominant driver changes in space throughout the year, with blooms of dominance for  $U$  in the desert Southwest during the warm season, for  $R_d$  in the humid Southeast in summer, and for  $q$  in the Atlantic states in late fall to winter. These seasonal variations in the relative strengths of the drivers were observed by other researchers, albeit in examinations of sensitivities alone, not complete variability analyses. Saxton (1975) found strong seasonal variation between the relative sensitivities of the aerodynamic and radiative components of daily reference ET in western Iowa, with net radiation being the most important driver year-round but the aerodynamic driver dominating in spring and fall. Piper (1989) found that reference ET in the tropics was most sensitive to  $T$  but that its effects varied seasonally. Irmak et al. (2006) also found significant hydroclimatic and seasonal variation in the sensitivity of reference ET to its drivers, although first to vapor pressure deficit and then to  $U$ .

The bottom panel of figure 8 shows the intra-annual cycle of the top-ranked drivers of daily  $ET_r$  variability. Clearly,  $T$  dominates in two modes: one in early spring (~97% of CONUS in March) and the other in fall (~88% in October and November). The area over which  $T$  dominates is smallest at the height of summer (~57% in July). This coincides with the bloom in the Southwest of  $U$  dominance (29% in August) and in the Southeast of  $R_d$  dominance (17% in July). In contrast,  $q$  reaches peak dominance during winter (~16% in January; the maps show that this is primarily in the Atlantic states). Also shown are the distributions of top-ranked drivers by area for daily variability across MJJASO and for annual variability (see figs. 7 and 10).

#### DECOMPOSING ANNUALLY ESTIMATED $ET_r$

Modeling  $ET_r$  at the annual timescale (i.e., using NLDAS-2 drivers that have been averaged across each year and thus represent annual values in daily units, so  $n = 30$ ) eliminates any effects on the decomposition of  $ET_r$  variability of strongly seasonal drivers and yields much simpler results with regard to the relative contributions to  $ET_r$  variability of each driver (fig. 9) and the top-ranked driver (fig. 10). Annually,  $B_T$  and  $B_q$  exhibit opposite patterns; where  $T$  makes its greatest contribution to  $ET_r$  variability (in northern and northeastern CONUS) and  $q$  tends to mitigate that variability, and vice-versa (in southern and southwestern CONUS).  $T$  dominates  $ET_r$  variability over the vast majority of CONUS, with few exceptions. While  $q$  does not dominate  $ET_r$  variability anywhere at the daily timescale, at the annual timescale  $q$  dominates in the arid Southwest, central and coastal California, and west Texas (places where  $U$  dominates daily  $ET_r$  variability) and in central Florida (where  $R_d$  dominates daily  $ET_r$  variability).  $U$  and  $R_d$  dominate in very small areas of far-southern Florida.

## DISCUSSION AND CONCLUSIONS

In this study, the variability observed in a 30-year ASCE05-derived, CONUS-wide  $ET_r$  reanalysis has been decomposed at various timescales and timeframes into contributions from each model driver, both acting independent-

ly and covarying with the other drivers. The application of the Method of Moments analysis was detailed, including the analytical expressions of the sensitivity of ASCE05-derived  $ET_r$  to its drivers, which, along with driver variances and covariances, were mapped across CONUS. In addition, each driver's relative contribution to  $ET_r$  variability was mapped and compared.

#### MAIN FINDINGS

With regard to the spatio-temporal distribution of the drivers' relative contributions to  $ET_r$  variability, the main qualitative result from this study is the demonstration of the volatility of dominant drivers in time and space. Such seasonal variations are also found across a variety of hydroclimates in CONUS (Saxton, 1975; Irmak et al., 2006). Most obvious here is the role of  $T$  as a driver of  $ET_r$  variability across all timescales examined, particularly across the northern continental interior.  $T$  is the top-ranked driver of variability across ~93% of CONUS at both the annual timescale and the daily timescale across MJJASO, which was also found in the tropics by Piper (1989), who stated that the accuracy in determining  $T$  was paramount. However, each driver's relative contributions reveal important regional and temporal caveats, as strong patterns emerge in the drivers' relative contributions across many timescales. At both the daily MJJASO and annual timescales,  $T$  dominates in the northern continental interior and the Northeast but is much less important in the Southwest. In contrast,  $q$  shows a strongly inverse pattern to  $T$ , with its greatest contribution in the Southwest and a negative contribution (i.e., reducing  $ET_r$  variability) in the Great Lakes region and Northeast. Across both of these timescales, the contribution of  $U$  is consistently at its strongest in the Southwest and weakly negative in the Northeast and Pacific Northwest (however, as noted below, when daily variability is examined on a month-by-month basis, a different pattern emerges).

Examining these results regionally reveals significant and distinct patterns, particularly in the Southwest and Southeast. At the daily timescale across both the MJJASO warm season and the summer months,  $U$  and  $R_d$  increase in rank in the Southwest and Southeast, respectively, where they become the dominant drivers, implying that they should be explicitly modeled in these regions at all timescales. Similarly,  $ET_r$  estimation must include a humidity driver at the daily timescale over the Eastern Seaboard, where humidity dominates daily  $ET_r$  variability in winter. Interestingly, the  $U$  dominance over the Southwest and the  $R_d$  dominance over the Southeast are not reproduced at the annual timescale; instead,  $q$  dominates annual variability here.

The Southwest/Southeast pattern generally mimics the distinction between water- and energy-limited hydroclimates across CONUS, an observation also supported by work at an oasis in western China (Hou et al., 2013). In the water-limited region of the Southwest, the strong linkage between the variabilities of  $U$  and  $ET_r$  may result from variations in the availability of water that dominate changes in  $ET_r$  that in turn result in complementary variations in  $ET_r$  through advective feedbacks at the land surface-atmosphere

interface. This is the complementary relationship between ET and evaporative demand (Bouchet, 1963). On the other hand, in energy-limited regions such as the Southeast, variations in energy availability (i.e., in  $R_d$ ) drive variations in ET and evaporative demand in parallel (Hobbins et al., 2004). The behaviors in the Southwest and Southeast represent extremes of a hydroclimatic continuum. Everywhere else lies somewhere in between, away from the strongest effects of  $U$  and  $R_d$ , where other drivers can dominate ET<sub>r</sub> variability. This hypothesis bears further examination that lies beyond the scope of this study.

There are also significant differences in a given driver's behavior between timescales.  $R_d$  shows different patterns between the daily and annual timescales.  $R_d$  makes very little contribution anywhere across CONUS at the annual timescale; however, at least in the Southeast,  $R_d$  makes the greatest contribution of all drivers at the daily timescale across MJJASO. The development of  $U$  dominance across the Southwest revealed by the month-to-month analysis of daily variability demonstrates that the pooling of daily data into MJJASO encodes a strong seasonality that tends to overstate the importance of  $T$ . The monthly breakdown removes this seasonality effect and uncovers the importance of all other drivers. In summer months,  $U$  dominates in the Southwest, and  $R_d$  dominates in the Southeast. In winter months,  $q$  dominates across the Eastern Seaboard. These findings demonstrate the strong (and often confounding) effects of drivers' implicit seasonality on variability analyses.  $T$  dominates at the daily timescale across MJJASO (top-ranked across 94.6% of CONUS) but less so for daily ET<sub>r</sub>; at the monthly breakdown, when the effects of the seasonality of  $T$  are less pronounced and other drivers dominate. At the annual timescale, the Eastern Seaboard dominance by  $q$  is not replicated; instead,  $q$  dominates in areas where  $U$  (in the Southwest) and  $R_d$  (in the Southeast) otherwise dominate at monthly timescales. This timescale-dependent behavior was also observed across a variety of far finer temporal scales in Belgium, where the most pronounced errors in ET<sub>r</sub> arose due to the sampling frequency of  $U$  and  $R_d$  (Hupet and Vanclooster, 2001).

## SOURCES OF ERROR AND FUTURE WORK

NOAA generates the ET<sub>r</sub> product examined here from a reanalysis dataset from a fully coupled land surface-atmosphere assimilation model. Nevertheless, following validation of NOAA ET<sub>r</sub> against 704 stations in agricultural areas of western CONUS (Lewis et al., 2014) and 18 agrometeorological stations in the TXHPET network (Moorhead et al., 2015), we conclude that, while NOAA ET<sub>r</sub> is suitable for use in regional water resources management, the following improvements are necessary before it is used for irrigation scheduling:

1. The input meteorological variables ( $T$ ,  $q$ , and  $U$ ) should be conditioned, i.e., they should be adjusted from values observed under ambient, non-reference conditions to better represent conditions that would apply over the theoretical reference surface assumed in the reference ET paradigm.
2. The reanalysis of wind speeds should be improved. While our results indicate a prominent role for  $U$  in

determining ET<sub>r</sub> variability in the desert Southwest, this might reflect the fact that wind speed is generally one of the most difficult meteorological variables to model. Lewis et al. (2014) found that NLDAS-2 hourly wind speeds exhibited the lowest correlation to station observations in southern parts of California, Arizona, and much of the Rocky Mountains.

3. The spatial resolution of drivers and predicted ET<sub>r</sub> should be improved. This could follow the example of Abatzoglou (2013), who combined the spatial attributes of a long-term climatological dataset from the Precipitation-elevation Regressions on Independent Slopes Model (PRISM; Daly et al., 1994) with the temporal attributes of the NLDAS-2 drivers used here to generate a finer-resolution (4 km) set of drivers suitable for ecological applications. As the Abatzoglou (2013) dataset is only available for 1979 to 2010, NOAA has not used it to generate its ET<sub>r</sub> product.

4. Any bias remaining in the drivers and the modeled ET<sub>r</sub> after steps 1 to 3 should be corrected.

NOAA plans to include such improvements in future generations of their ET<sub>r</sub> product. As this study examined variations of drivers and response variables that have been shown to be strongly correlated with observations (Lewis et al., 2014; Moorhead et al., 2015), these error sources are unlikely to have altered the findings of this analysis, and so we remain confident in our conclusions. Further, the application of the FOSM technique still applies as described (eqs. 4 and 5), as do the sensitivity equations (eqs. 6 to 10), regardless of whether or not further improvements are made to the ET<sub>r</sub> reanalysis.

## TEMPERATURE-BASED EVAPORATIVE DEMAND WARNING

The  $T$ - $R_d$  assumption that underpins  $T$ -based parameterizations of evaporative demand used in much (flawed) hydrologic practice holds that, due to a positive covariance between  $T$  and  $R_d$ , the variability of the  $R_d$  driver can be replicated by some parameterization of  $T$ , as surface heating follows from clearer skies and surface cooling follows from increasing cloudiness. However, there are many regions or seasons of negative covariance between  $T$  and  $R_d$ . For example, in the Southeast, not only will relying on the  $T$ - $R_d$  assumption at the monthly timeframe result in errors (Hobbins et al., 2012), but these errors will be exacerbated by the failure to explicitly represent the increased regional variability of  $R_d$ . Our results are predicated on our choice of a physically based ET<sub>r</sub> parameterization and its full suite of drivers (and their sensitivities), which should lead to a smaller effect of  $T$  as a driver of ET<sub>r</sub> variability as compared to  $T$ -based parameterizations. It is therefore interesting to note the persistence of nearly CONUS-wide dominance of  $T$  as a driver of annual ET<sub>r</sub> variability. While this dominance appears to support the use of  $T$ -based formulations of evaporative demand, e.g., Thornthwaite (1948), Hargreaves (Hargreaves and Samani, 1985), Hamon (1961), and Blaney-Criddle (USDA, 1950), it must be emphasized that this result only applies to ET<sub>r</sub> estimated from annual drivers.  $T$  is not always the most significant driver

of temporal variability in ASCE05 ET<sub>r</sub> in particular nor of physically based evaporative demand in general (Hobbins et al., 2012) at intra-annual timescales. Instead, the dominant drivers of ET<sub>r</sub> variability depend on timescale, timeframe, and region. Only across a very small area of the upper Midwest is *T* always the dominant variable driving ET<sub>r</sub> variability; it is never the top-ranked driver everywhere.

Unfortunately, many operational users of parameterizations of evaporative demand remain unaware of the assumptions of *T*-based models, or even that they may be using one at all, as such parameterizations are often embedded within other models of the land surface. As an example of the dangers of this practice, Hobbins et al. (2008) and Sheffield et al. (2012) showed that the *T*-based parameterization of evaporative demand that drives ET in the Palmer Drought Severity Index (PDSI) overestimates trends in droughtiness. In summary, depending on region, season, and timescale, drivers other than *T* dominate. Thus, we conclude that *T*-driven models of evaporative demand are not recommended for any season at all points, or for all seasons at most points.

#### **PARSIMONY VS. PHYSICAL REPRESENTATIVENESS**

While we may *a priori* prefer models that are physically based, practice may force a different model upon us, with the choice predicated on a trade-off between the desired physical representativeness and the increased uncertainty that results from addition of more variables and parameters. Driver selection is crucial to provide accurate results at time and space scales relevant to operational goals and to avoid both extraneous modeling uncertainty or the omission of key sources of variability. Understanding what drives the variability of a physically based estimate of ET<sub>r</sub>, and by extension evaporative demand in general, by decomposition of the variability into its drivers at appropriate regional and temporal scales is essential for operational hydrologists and agriculturalists seeking this balance. It permits users to prioritize efforts to reduce uncertainty in the most significant drivers, make the most appropriate model selection, and evaluate model parameters.

While the choice of model used here (the ASCE Standardized Reference Evapotranspiration Equation) locked in the driver set and therefore the sensitivities to the drivers, this parameterization is widely accepted as representative of physically based models of ET<sub>r</sub>, in particular and, indeed, evaporative demand in general.

#### **ACKNOWLEDGEMENTS**

The NLDAS-2 data used were acquired as part of the mission of NASA's Earth Science Division and archived and distributed by the Goddard Earth Sciences Data and Information Services Center. The author was supported by the National Integrated Drought Information System (NIDIS) and Inter-Agency Agreement No. AID-FFP-P-10-00002/006 between USAID and NOAA for support to the Famine Early Warning Systems Network (FEWS NET).

#### **REFERENCES**

- Abatzoglou, J. T. (2013). Development of gridded surface meteorological data for ecological applications and modeling. *Int'l. J. Climatol.*, 33(1), 121-131.  
<http://dx.doi.org/10.1002/joc.3413>.
- ASCE. (2005). The ASCE standardized reference evapotranspiration equation. Task Committee on Standardization of Reference Evapotranspiration. Reston, Va.: ASCE Water Resources Institute.
- Bouchet, R. J. (1963). Évapotranspiration réelle et potentielle, signification climatique. *Proc. Int'l. Assoc. Scientific Hydrol.* (pp. 134-142). Publication No. 62. Wallingford, U.K.: IAHS Press. Retrieved from [http://iahs.info/uploads/dms/iahs\\_062\\_0134.pdf](http://iahs.info/uploads/dms/iahs_062_0134.pdf).
- Daly, C., Neilson, R. P., & Phillips, D. L. (1994). A statistical-topographic model for mapping climatological precipitation over mountainous terrain. *J. Appl. Meteorol.*, 33(2), 140-158.  
[http://dx.doi.org/10.1175/1520-0450\(1994\)033<0140:ASTMFM>2.0.CO;2](http://dx.doi.org/10.1175/1520-0450(1994)033<0140:ASTMFM>2.0.CO;2).
- Doorenbos, J., & Pruitt, W. O. (1984). Crop water requirements. Irrigation and Drainage Paper No. 24 (Revised). Rome, Italy: United Nations FAO.
- FAO. (1998). Crop evapotranspiration: Guidelines for computing crop water requirements. Irrigation and Drainage Paper No. 56. Rome, Italy: United Nations FAO.
- Fisher, J. B., DeBiase, T. A., Qi, Y., Xu, M., & Goldstein, A. H. (2005). Evapotranspiration models compared on a Sierra Nevada forest ecosystem. *Environ. Model. Software*, 20(6), 783-796.  
<http://dx.doi.org/10.1016/j.envsoft.2004.04.009>.
- Fisher, J. B., Tu, K. P., & Baldocchi, D. B. (2008). Global estimates of the land-atmosphere water flux based on monthly AVHRR and ISLSCP-II data, validated at 16 FLUXNET sites. *Remote Sensing Environ.*, 112(3), 901-919.  
<http://dx.doi.org/10.1016/j.rse.2007.06.025>.
- Goyal, R. K. (2004). Sensitivity of evapotranspiration to global warming: A case study of arid zone of Rajasthan (India). *Agric. Water Mgmt.*, 69(1), 1-11.  
<http://dx.doi.org/10.1016/j.agwat.2004.03.014>.
- Ham, C., Hobbins, M. T., Abt, K. L., & Prestemon, J. P. (2014). Using the evaporative demand drought index and the Palmer drought severity index to forecast the number of large wildland fires on federal lands. Presented at the Large Wildland Fires Conference, Missoula, Montana.
- Hamon, W. R. (1961). Estimating potential evapotranspiration. *J. Hydraulics Div. ASCE*, 87 (HY3), pp. 107-120.
- Hargreaves, G. H., & Samani, Z. A. (1985). Reference crop evapotranspiration from temperature. *Appl. Eng. Agric.*, 1(2), 96-99. <http://dx.doi.org/10.13031/2013.26773>.
- Hobbins, M. T., Ramírez, J. A., & Brown, T. C. (2004). Trends in pan evaporation and actual evapotranspiration across the conterminous U.S.: Paradoxical or complementary? *Geophys. Res. Letters*, 31(13), L13503.  
<http://dx.doi.org/10.1029/2004GL0198426>.
- Hobbins, M. T., Dai, A., Roderick, M. L., & Farquhar, G. D. (2008). Revisiting the parameterization of potential evaporation as a driver of long-term water balance trends. *Geophys. Res. Letters*, 35(12), L12403.  
<http://dx.doi.org/10.1029/2008GL033840>.
- Hobbins, M. T., Wood, A., Streubel, D., & Werner, K. (2012). What drives the variability of evaporative demand across the conterminous U.S.? *J. Hydrometeorol.*, 13(4), 1185-1214.  
<http://dx.doi.org/10.1175/JHM-D-11-0101.1>.
- Hobbins, M. T., Wood, A., McEvoy, D. J., Huntington, J. L., Morton, C., Verdin, J., Anderson, M., & Hain, C. (2016). The evaporative demand drought index: Part I. Linking drought evolution to variations in evaporative demand. *J. Hydrometeorol.* (in press).

- Hou, L.-G., Zou, S.-B., Xiao, H.-L., & Yang, Y.-G. (2013). Sensitivity of the reference evapotranspiration to key climatic variables during the growing season in the Ejina oasis northwest China. *Springer Plus* 2(supp. 1): S1-S4. <http://dx.doi.org/10.1186/2193-1801-2-S1-S4>.
- Hupet, F., & Vanclooster, M. (2001). Effect of the sampling frequency of meteorological variables on the estimation of the reference evapotranspiration. *J. Hydrol.*, 243(3-4), 192-204. [http://dx.doi.org/10.1016/S0022-1694\(00\)00413-3](http://dx.doi.org/10.1016/S0022-1694(00)00413-3).
- Irmak, S., Payero, J. O., Martin, D. L., Irmak, A., & Howell, T. A. (2006). Sensitivity analyses and sensitivity coefficients of standardized daily ASCE-Penman-Monteith equation. *J. Irrig. Drain. Eng.*, 132(6), 564-578. [http://dx.doi.org/10.1061/\(ASCE\)0733-9437\(2006\)132:6\(564\)](http://dx.doi.org/10.1061/(ASCE)0733-9437(2006)132:6(564)).
- Jensen, M. E., & Haise, H. R. (1963). Estimating evapotranspiration from solar radiation. *J. Irrig. Drain. Eng. Div. ASCE*, 89(IR4), 15-41.
- Lewis, C. S., Geli, H. M. E., & Neale, C. M. U. (2014). Comparison of the NLDAS weather forcing model to agrometeorological measurements in the western U.S. *J. Hydrol.*, 510, 385-392. <http://dx.doi.org/10.1016/j.jhydrol.2013.12.040>.
- McCuen, R. H. (1974). A sensitivity and error analysis of procedures used for estimating evapotranspiration. *Water Resour. Bull.*, 10(3), 486-498. <http://dx.doi.org/10.1111/j.1752-1688.1974.tb00590.x>.
- Mishra, S. (2009). Uncertainty and sensitivity analysis techniques for hydrologic modeling. *J. Hydroinformatics*, 11(3-4), 282-296. <http://dx.doi.org/10.2166/hydro.2009.048>.
- Mitchell, K. E., Lohmann, D., Houser, P. R., Wood, E. F., Schaake, J. C., Robock, A., Cosgrove, B. A., Sheffield, J., Duan Q., Luo, L., Higgins, R. W., Pinker, R. T., Tarpley, J. D., Lettenmaier, D. P., Marshall, C. H., Entin, J. K., Pan, M., Shi, W., Koren, V., Meng, J., Ramsay, B. H., & Bailey, A. A. (2004). The multi-institution North American Land Data Assimilation System (NLDAS): Utilizing multiple GCIP products and partners in a continental distributed hydrological modeling system. *J. Geophys. Res.*, 109(D7), D07S90. <http://dx.doi.org/10.1029/2003JD003823>.
- Monteith, J. L. (1965). Evaporation and environment. *Symp. Soc. Exp. Biol.*, 19, 205-234.
- Moorhead, J., Gowda, P., Hobbins, M. T., Senay, G., Paul, G., Marek, T., & Porter, D. (2015). Accuracy assessment of NOAA's gridded daily reference evapotranspiration for the Texas High Plains. *J. American Water Resour. Assoc.*, 51(5), 1262-1271. <http://dx.doi.org/10.1111/1752-1688.12303>.
- NWS. (2015). Forecast reference evapotranspiration. Washington, D.C.: National Weather Service. Retrieved from <http://preview.weather.gov/graphical/?zoom=4&lat=37&lon=-96.5&layers=F000BTTFTT>.
- Penman, H. L. (1948). Natural evaporation from open water, bare soil, and grass. *Proc. Royal Soc. London A*, 193(1032), 120-145.
- Penman, H. L. (1963). Vegetation and hydrology. Technical Communication 53. Harpenden, U.K.: Commonwealth Bureau of Soils. <http://dx.doi.org/10.1097/00010694-196311000-00014>.
- Piper, B. S. (1989). Sensitivity of Penman estimates of evaporation to errors in input data. *Agric. Water Mgmt.*, 15(3), 279-300. [http://dx.doi.org/10.1016/0378-3774\(89\)90021-8](http://dx.doi.org/10.1016/0378-3774(89)90021-8).
- Saxton, K. E. (1975). Sensitivity analyses of the combination evapotranspiration equation. *Agric. Meteorol.*, 15(3), 343-353. [http://dx.doi.org/10.1016/0002-1571\(75\)90031-X](http://dx.doi.org/10.1016/0002-1571(75)90031-X).
- Sheffield, J., Wood, E. F., & Roderick, M. L. (2012). Little change in global drought over the past 60 years. *Nature*, 491(7424), 435-438. <http://dx.doi.org/10.1038/nature11575>.
- Thornthwaite, C. W. (1948). An approach toward a rational classification of climate. *Geogr. Rev.*, 38(1), 55-94. <http://dx.doi.org/10.2307/210739>.
- Turc, L. (1961). Evaluation des besoins en eau d'irrigation, évapotranspiration potentielle. *Annales Agronomiques*, 12(1), 13-49.
- USDA. (1950). Determining water requirements in irrigated areas from climatological and irrigation data. Tech. Paper No. 96. Washington, D.C.: USDA Soil Conservation Service.
- Xia, Y., Mitchell, K., Ek, M., Sheffield, J., Cosgrove, B., Wood, E., Luo, L., Alonge, C., Wei, H., Meng, J., Livneh, B., Lettenmaier, D., Koren, V., Duan, Q., Mo, K., Fan, Y., & Mocko, D. (2012). Continental-scale water and energy flux analysis and validation for the North American Land Data Assimilation System project phase 2 (NLDAS-2): 1. Intercomparison and application of model products. *J. Geophys. Res. Atmos.*, 117(D3), D03109. <http://dx.doi.org/10.1029/2011JD016048>.